Molecular Cancer Therapeutics

Identification of Cancer-Targeted Tropomyosin Inhibitors and Their Synergy with Microtubule Drugs

Mark A. Currier[1,2], Justine R. Stehn[3,4], Ashleigh Swain[3], Duo Chen[1], Jeff Hook[3], Eleanor Eiffe[4], Andrew Heaton[3,4], David Brown[3,4], Brooke A. Nartker[1], David W. Eaves[5], Nina Kloss[3], Herbert Treutlein[6], Jun Zeng[7], Irina B. Alieva[3,8], Vera B. Dugina[3,9], Edna C. Hardeman[3], Peter W. Gunning[3], and Timothy P. Cripe[1,2]

Abstract

Actin filaments, with their associated tropomyosin polymers, and microtubules are dynamic cytoskeletal systems regulating numerous cell functions. While antimicrotubule drugs are well-established, antiactin drugs have been more elusive. We previously targeted actin in cancer cells by inhibiting the function of a tropomyosin isoform enriched in cancer cells, Tpm3.1, using a first-in-class compound, TR100. Here, we screened over 200 other antitropomyosin analogues for anticancer and on-target activity using a series of *in vitro* cell-based and biochemical assays. ATM-3507 was selected as the new lead based on its ability to disable Tpm3.1-containing filaments, its cytotoxicity potency, and more favorable drug-like characteristics. We tested ATM-3507 and TR100 alone and in combination with antimicrotubule agents against neuroblastoma models *in vitro* and *in vivo*. Both ATM-3507 and TR100 showed a high degree of synergy *in vitro* with vinca alkaloid and taxane antimicrotubule agents. *In vivo*, combination-treated animals bearing human neuroblastoma xenografts treated with antitropomyosin combined with vincristine showed minimal weight loss, a significant and profound regression of tumor growth and improved survival compared with control and either drug alone. Antitropomyosin combined with vincristine resulted in G_2–M phase arrest, disruption of mitotic spindle formation, and cellular apoptosis. Our data suggest that small molecules targeting the actin cytoskeleton via tropomyosin sensitize cancer cells to antimicrotubule agents and are tolerated together *in vivo*. This combination warrants further study. *Mol Cancer Ther; 16(8); 1555–65. ©2017 AACR.*

Introduction

High-risk neuroblastoma is responsible for 10%–15% of pediatric cancer mortality. Vinca alkaloids, such as vincristine, which disrupt assembly of tubulin monomers into microtubules, are foundational in chemotherapeutic regimens used to treat patients with neuroblastoma. Despite aggressive treatment with chemotherapy, surgery, radiation, high-dose chemotherapy with autologous stem cell rescue, anti-GD2 immunotherapy, and retinoic acid, about 50% of children with high-risk neuroblastoma experience disease relapse. Children with relapsed/refractory neuroblastoma have a <10% chance of survival (1). In addition, an increasing number of neuroblastoma survivors develop multisystem deficiencies (2) and secondary malignancies (3) as a result of the toxic chemotherapy exposures. Thus, novel therapies are urgently needed for these children.

The actin cytoskeleton has long been regarded as an attractive target for cancer therapy, but the intolerable cardiotoxicity associated with targeting actin has resulted in a lack of antiactin agents passing through animal toxicity (4–8). In metazoans, actin filaments are usually formed as a copolymer with tropomyosin where the particular isoform of tropomyosin defines the functional properties of the filament (9). The tropomyosin isoform Tpm3.1 (previously known as Tm5NM1) is of particular interest as it is one of only two tropomyosins retained by essentially all tumor cells and is structurally divergent from the muscle tropomyosins (10, 11). We previously reported a novel anticancer strategy based on disrupting actin filaments containing Tpm3.1 by targeting this tropomyosin isoform (12). The tool compound we used, TR100 (Fig. 1), was identified by an *in silico* small-molecule screening strategy for binding to a pocket in the C-terminus of Tpm3.1. We found that TR100 destabilized actin filaments

[1]Center for Childhood Cancer and Blood Diseases, Nationwide Children's Hospital, Columbus, Ohio. [2]Division of Hematology/Oncology/Blood and Marrow Transplantation, Nationwide Children's Hospital, Columbus, Ohio. [3]School of Medical Sciences, University of New South Wales Australia, Sydney, New South Wales, Australia. [4]Novogen Pty Ltd, Hornsby, New South Wales, Australia. [5]Division of Oncology, Cincinnati Children's Hospital Medical Center, Cincinnati, Ohio. [6]Sanoosa Pty. Ltd., Melbourne, Victoria, Australia. [7]MedChemSoft Solutions, Wheelers Hill, Victoria, Australia. [8]Department of Electron Microscopy, A. N. Belozersky Institute of Physico-Chemical Biology, Lomonosov Moscow State University, Moscow, Russia. [9]Mathematical Methods in Biology, A.N. Belozersky Institute of Physico-Chemical Biology, Lomonosov Moscow State University, Moscow, Russia.

Note: Supplementary data for this article are available at Molecular Cancer Therapeutics Online (http://mct.aacrjournals.org/).

Corresponding Author: Timothy P. Cripe, Division of Hematology/Oncology/BMT, Nationwide Children's Hospital, 700 Children's Dr, Columbus, OH 43205. Phone: 614-722-3552; Fax: 614-722-3699; E-mail: Timothy.Cripe@nationwidechildrens.org

doi: 10.1158/1535-7163.MCT-16-0873

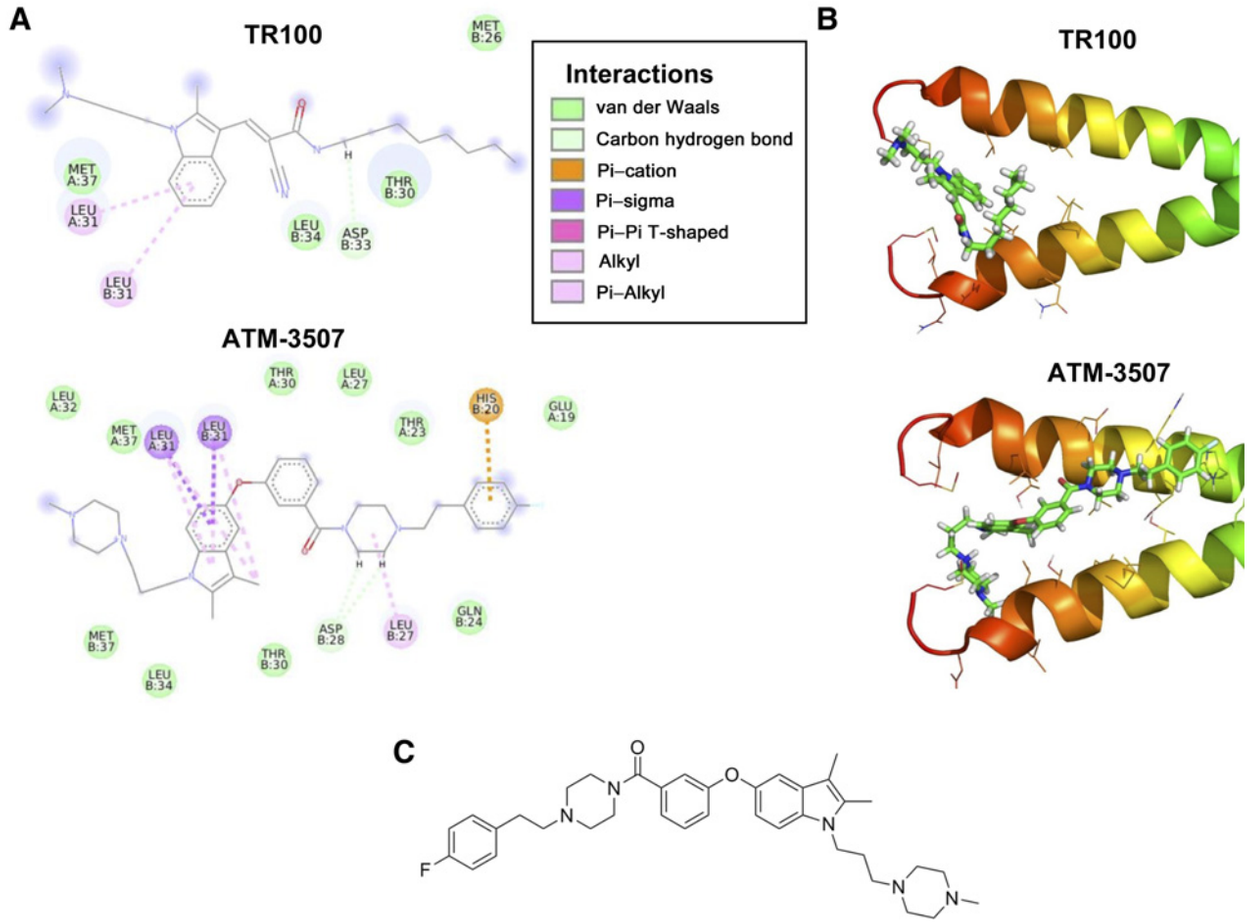

Figure 1.
Molecular structural diagrams of small-molecules (**A**) binding the tropomyosin C-terminus (**B**). The predicted molecular interactions between the tropomyosin C-terminus and both the tool compound, TR100, and lead compound, ATM-3507, are shown. Compared with TR100, the more linear shape of ATM-3507 can form more contacts with Tpm3.1 residues resulting in a higher binding affinity. ATM-3507 also extends into an area on tropomyosin with less conserved side chains (**B**, right) thereby allowing increased specificity of the compound. For example, HIS B 20 in **A** is specific to Tpm3.1 and Tpm3.2. The glutamic acid at the C-terminus of Tpm3.1 increases its negative charge and it is therefore essential for the inhibitor to include a positive partial charge. **C**, Two-dimensional diagram of the ATM-3507 chemical structure.

containing Tpm3.1 both in cell culture models and also in pure actin filaments *in vitro* (12). Furthermore, we showed TR100 is cytotoxic for numerous cancer cell lines and induces a delayed growth pattern in several tumor models, including CHP134 human neuroblastoma xenografts. The lack of any objective clinical responses in these studies, however, suggested a need for a more potent lead compound for combination therapy.

Microtubules are also important regulators of cell division and intracellular transport, and a key target in cancer cells. Here we sought to identify a better antitropomyosin drug candidate and to determine whether simultaneously targeting both the actin cytoskeleton and microtubules is an effective anticancer strategy. Following an extensive *in vitro* screen, we selected ATM-3507 as a potent antitropomyosin inhibitor. To validate ATM-3507, we tested both TR100 (tool compound) and ATM-3507, alone and in combination with antimicrotubule drugs, in neuroblastoma models. We found a strong synergistic effect on cell lines and in animal xenografts. Targeting these important cytoskeletal systems induced profound G_2–M arrest, disruption of the mitotic spindle, and cellular apoptosis.

Materials and Methods

Compounds and reagents

TR100 and ATM-3507 were synthesized as described previously (13 and 14, respectively) and ATM-3507 was patented (14). The lead antitropomyosin, ATM-3507, was provided by Novogen. Paclitaxel, vincristine, doxorubicin, and etoposide were purchased from Sigma-Aldrich; vincristine was also purchased from Selleck Chemicals. The general caspase inhibitor Z-VAD-FMK was acquired from Calbiochem. For *in vitro* studies, each of the above compounds were dissolved in dimethyl sulfoxide (DMSO, Sigma Aldrich) at 50 mmol/L and then diluted to the appropriate concentrations in complete media. DMSO alone was diluted in complete media as a control for the *in vitro* assays. In some experiments, vincristine was diluted in PBS. The sources of antibodies are mentioned in Supplementary Material.

Cell lines and cultures

Media used for cell cultures and cell viability assays are described in Supplementary Material. Human neuroblastoma cell lines CHLA-20, SK-N-BE(2), SK-N-SH, and SH-SY5Y were kind gifts from Thomas Inge (Cincinnati Children's Hospital, Cincinnati, OH) in September of 2002. The human neuroblastoma cell line CHP-134 was a kind gift from the laboratory of Timothy Crombleholme (Cincinnati Children's Hospital, Cincinnati, OH) in December 2006. The human neuroblastoma cell line CHLA-90 was requested from the Pediatric Preclinical Testing Program (PPTP, http://gccri.uthscsa.edu/pptp) in September of 2013. These six cell lines were verified by short tandem repeat genotyping in January 2013 and tested negative for mycoplasma prior to experimental use. Both SKMEL-28 and PC3 were obtained from the ATCC in 2007. These two lines were not authenticated but were tested for mycoplasma using the MycoAlert detection kit (Lonza) in February, 2014.

Compound library screen

The activity of approximately 200 antitropomyosin analogues was assessed against a panel of eight cell lines representing a range of cancer types. Data are shown in Fig. 2A for the melanoma cell line SK-MEL-28 and the prostate cancer cell line PC3. The compound library was generated using a structure-based design approach to target the C-terminal domain of tropomyosin Tpm3.1. A Versatile Approach to Library-Based Iterative Design "VAL-ID" was employed to generate a variety of analogues based on a substituted indole scaffold. *In vitro* cytotoxicity of the compounds was assessed using CellTiter-Glo Luminescent Cell Viability Assay. Cells were plated in 96-well plates at 3,000–5,000 cells per well, incubated at 37 °C overnight, and then treated with various concentrations of the test compounds. The cells were incubated in the presence of test compounds for 72 hours at 37°C, after which the cells were exposed to Cell-Titer Glo reagent for 30 minutes. Luminescence was captured using an EnVision multilabel reader and the data for each analogue concentration compared against no treatment control. Inhibitory concentration $(IC)_{50}$ values were calculated as drug concentrations necessary to inhibit 50% growth compared with untreated control cells.

Molecular modeling

For the prediction and modeling of the binding mode of ATM-3507 to Tpm3.1 we applied a method similar to the one described previously (12). A homology model of Tpm3.1 was first built based on the solution NMR structure of the junction between tropomyosin molecules (15). The coordinates for the NMR structures were obtained from the PDB databank (16), PDB id 2g9j and a representative structure was chosen out of the 10 NMR models as the template structure. The homology model was created using SWISS-MODEL (17); however, the helical conformation and side

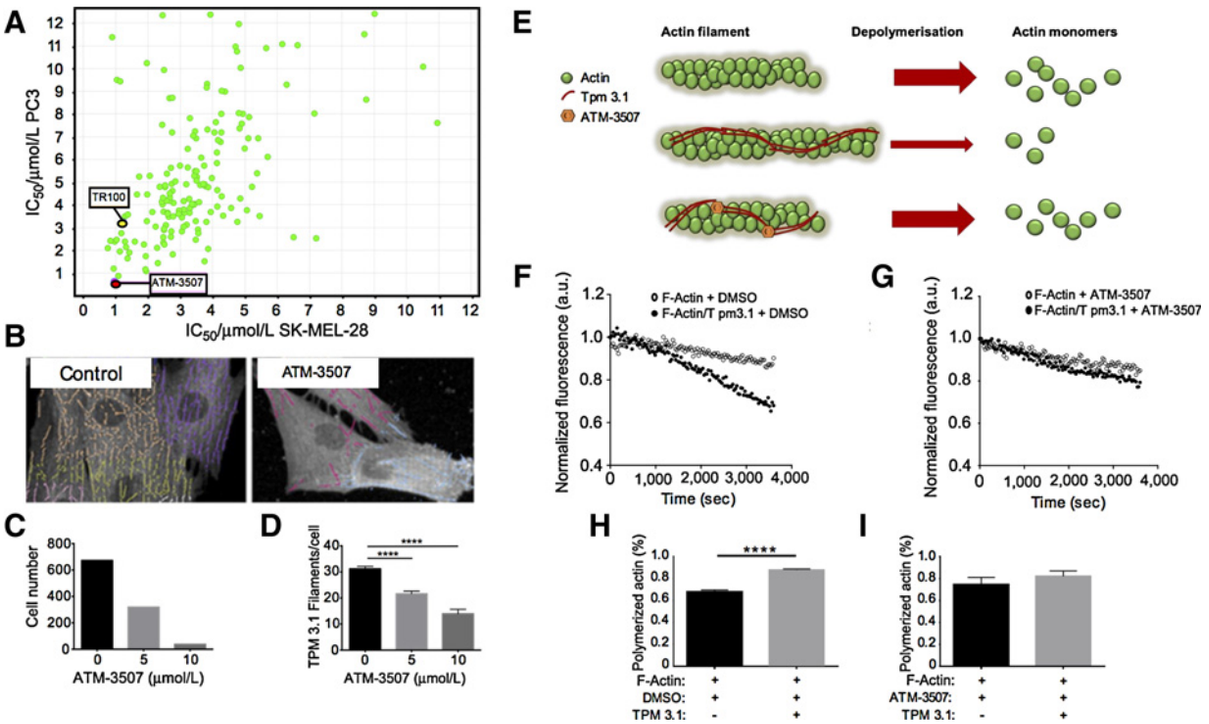

Figure 2.

Lead antitropomyosin ATM-3507 binds to and impairs Tpm3.1 function inducing cancer cell death *in vitro*.**A**, A representative scatter plot displaying the distribution of activity (IC_{50}, μmol/L) of antitropomyosin analogues. Highlighted are lead ATM-3507 and first-in-class TR100. **B**, ATM-3507 impact on Tpm3.1 filaments was quantitated in SKN-SH cells using a HCI assay in combination with the Commonwealth Scientific and Industrial Research Organization linear feature detection algorithm. Cell number (**C**) and Tpm3.1 filaments/cell area (**D**; μm^2) were quantitated using >300 cells ($n = 3$ independent experiments; ****, $P < 0.0001$). **E**, Schematic of ATM-3507 mechanism of action. **F**, Depolymerization time course of actin filaments (35% pyrene labeled) in the presence or absence of saturating amounts of Tpm3.1. **G,** Tpm3.1 was preincubated with 50 μmol/L ATM-3507 or 1% (v/v) DMSO prior to mixing with F-actin. Depolymerization data is normalized to the initial fluorescence value. **H** and **I,** Quantitation of percent polymerized actin (mean ± SEM, $n > 6$ replicates; ****, $P < 0.0001$).

chain packing were optimized using a simulated annealing procedure based on Smith and colleagues (18) using NAMD2 (19).

The binding site available for ATM-3507 on the Tpm3.1 dimer was examined using a "Multiple Copy Simultaneous Search" (MCSS) method (20) where the preferred positions of 400 indole rings representing the scaffold of ATM-3507 were determined computationally around the C-terminus of Tpm3.1. Ten indole fragment clusters were found to be located inside the cavity of the C-terminus formed between two helices. These clusters then served as guidance for docking of ATM-3507 to the C-terminus. Our software "Qu-Cbit" (version 3.01, MedChemSoft Solutions, 2013) was used for the MCSS and docking calculations. Four conformations were selected followed by further refinement at quantum mechanical level. The QM calculations applied the GAMESS program (http://www.msg.ameslab.gov/gamess) to a system consisting of the ATM-3507 scaffold and ten Tpm3.1 residues surrounding the ligand. The QM calculations optimized the geometry of ATM-3507 with the protein residues kept fixed. Density Functional Theory method was applied using the B3LYP functional (21, 22) and the 6-31G(d) basis set (23). The conformation with the lowest total energy was selected as the best binding mode of the ATM-3507 scaffold. Using the optimized structure of the scaffold, the missing parts of ATM-3507 were added, followed by QM refinement of the geometry of the full ATM-3507 with the fixed residues of Tpm3.1.

Tpm3.1 filament quantitation

SK-N-SH neuroblastoma cells were seeded at 1,800 cells/well in a 384 Perkin Elmer High Content Imaging "Cell Carrier" plate and left to plate down 24 hours prior to treatment. Cells were then treated with 0–10 μmol/L ATM-3507. Twenty-four hours post-treatment, cells were fixed with 4% paraformaldehyde (PBS), permeabilized with Triton-X-100, and stained with γ9d (mouse mAb, 1:100) followed by GAM-488-conjugated secondary antibody (1:1,000) and DAPI to visualize the Tpm3.1-containing filament bundles and the nucleus, respectively. Supplementary Figure S1 shows that the mouse mAb γ9d used in this study recognizes only Tpm3.1/3.2 in these cells and has been thoroughly characterized in Schevzov and colleagues (11). Single-plane images were obtained on the Perkin Elmer Opera confocal microscope using a 20× objective. Twelve fields of view per condition (representing approximately 300–800 cells) were imaged. Changes in the number and length of Tpm3.1 filament bundles within each cell were quantitated using a linear feature detection algorithm developed by the Commonwealth Scientific and Industrial Research Organisation as described previously (24).

Actin depolymerization assay

A 12-μmol/L solution of labeled F-actin was prepared by polymerizing the monomeric actin (35% pyrene labeled Rabbit Muscle (Actin catalog no. AP05–Cytoskeleton Inc) into filaments in the presence of buffers A-Mg (2 mmol/L Tris HCl pH 8.0; 0.2 mmol/L $MgCl_2$; 0.2 mmol/L ATP; 0.5 mmol/L DTT) and T (100 mmol/L NaCl; 10 mmol/L Tris HCl pH 7.5; 2 mmol/L $MgCl_2$; 1 mmol/L EGTA; 0.5 mmol/L DTT) for 1 hour in the dark at room temperature. Tpm3.1 (10 μmol/L) was reduced in buffer T containing 1 mmol/L DTT at 56°C for 5 minutes and centrifuged at 135,000 × *g* for 30 minutes using a Hitachi Ultra Microcentrifuge to remove nonreduced dimers. Prior to the addition to polymerized pyrene-labeled F-actin (3 μmol/L), Tpm3.1 dimers (5 μmol/L) were incubated (10 minutes, room temperature) with or without 50 μmol/L of ATM-3507. The F-actin/Tpm3.1 ± ATM-3507 was incubated for 30 minutes at room temperature and samples were then transferred to a black walled 96-well plate. Duplicate samples were diluted 12-fold using an F-actin polymerization buffer (100 mmol/L NaCl; 10 mmol/L Tris HCl pH 7; 2 mmol/L $MgCl_2$; 1 mmol/L EGTA; 0.2 mmol/L ATP; 0.5 mmol/L DTT) and the polymerization rates of F-actin alone, F-actin/Tpm3.1, and the F-actin/Tpm3.1/ATM-3507 filament complex were measured using a Perkin Elmer EnSpire fluorescence plate reader (407 nm) at 30-second intervals for 60 minutes at room temperature. Data were normalized to the initial fluorescence value and polymerization curves of duplicate samples were fitted to a linear regression model using GraphPad Prism 6. Percent polymerization was determined at t_{60} as a function of t_0 (100%) for $n = 3$ independent experiments.

Animal studies

Animal studies were approved by the Institutional Animal Care and Use Committee for the Research Institute at Nationwide Children's Hospital. Female athymic nude mice, age 4–6 weeks, were purchased from Harlan Sprague Dawley. Mice were subcutaneously injected with 5.0×10^6 CHLA-20 cells in a 150 μL mix of PBS and Matrigel (2:1). For *in vivo* studies, ATM-3507 and TR100 were formulated at 15 mg/mL in 30% sulfobutyl-ether-β-cyclodextrin sodium salt (SBECD). Vincristine was dissolved in H_2O at 0.125 mg/kg. When the tumors reached volumes of 200–400 mm^3, mice were randomized into the study groups. Animals were followed until the animal reached endpoint criteria, including tumor volume >2,000 mm^3, body weight loss >20%, unusual mouse behavior, lack of movement, or poor posture. Tumor size was measured using digital calipers twice per week and tumor volume was calculated using the following formula: $a \times b^2(\pi/6)$ where "*a*" is the longest diameter and "*b*" is the shortest diameter. Mice were also weighed and observed twice per week for signs of endpoint condition. Mice that demonstrated signs of toxicity or reached endpoint criteria were humanely euthanized by CO_2 asphyxiation and subjected to cervical dislocation as the secondary method of euthanasia.

Immunofluorescence microscopy

Cell lines were cultured on coverslips coated with poly-D-lysine, and treated with TR100 ± vincristine or ATM-3507 ± vincristine at doses that had minimal impact alone but which in combination resulted in greater than 50% cell death. Twenty-four hours following treatment, coverslips were fixed using one of two methods. Coverslips used for analyzing the extent of chromatin condensation were briefly washed in 37°C serum-free media containing 20 mmol/L 2-[4-(2-hydroxyethyl)piperazin-1-yl]ethanesulfonic acid and fixed in 1% paraformaldehyde/wash medium for 15 minutes. The coverslips were then washed for 5 minutes in PBS at room temperature and fixation was completed using ice-cold methanol for 5 minutes, after which the methanol was steadily diluted out with PBS. Alternatively, coverslips used for imaging the microtubule network were fixed only in ice-cold methanol for 5 minutes, after which the methanol was steadily diluted out with PBS. The coverslips were stained with the primary antibody diluted in 2.5% FBS/PBS for 1 hour at room temperature: (α-tubulin: 1/300). The coverslips were then washed 3× for 10 minutes in PBS, and incubated with the secondary antibody diluted in 2.5% FBS/PBS for 30 minutes at room temperature in the dark (GAM-488: 1/500). The coverslips were again washed thrice for

10 minutes in PBS. 4′,6-Diamidino-2-phenylindole (DAPI) was included in the second PBS wash at 1/20,000, and following the final wash the coverslips were mounted using either Prolong Gold reagent (Life Technologies Inc.) or Aqua-Poly/Mount (Polysciences, Inc.). Imaging was carried out on a Leica TCS SP5 confocal microscope (Leica Microsystems Inc.), a Zeiss LSM 880 confocal microscope, and an Axioskop 40 epi-fluorescence microscope (Carl Zeiss Microscopy).

Cell-cycle analysis

Subconfluent human neuroblastoma cell lines treated with TR100 (3.1 μmol/L) ± vincristine (62.5 nmol/L for CHLA-20; 1.25 nmol/L for SKNBe2) or ATM-3507 (4 μmol/L) ± vincristine (10 nmol/L for CHLA-20; 1.5 nmol/L for SKNBe2) were harvested at the indicated time points (0.025% Trypsin-EDTA), washed in ice-cold PBS and then fixed in ice-cold ethanol for 1 hour at 4°C. After two washes in cold PBS, cellular DNA was stained with a propidium iodide (PI) solution (50 μg/mL PI and 0.1 mg/mL RNase A in PBS) for 30 minutes at room temperature. The percentage of cells in the G_0–G_1, S, and G_2–M phases was assessed using flow cytometry. The cell-cycle analyses were performed with FlowJo software (Tree Star, Inc.) or with the Guava Flow Cytometer (Merck Millipore) and analyzed with Incyte 2.1 software.

Quantitation of apoptotic cells

Subconfluent CHLA-20 cell cultures were treated with TR100 (4 μmol/L), ATM-3507 (4 μmol/L), vincristine (10 nmol/L) or the combination of TR100 plus vincristine or ATM-3507 plus vincristine for 6, 20, and 30 hours. Cells were then harvested, washed twice with cold PBS, and stained using the Annexin V-FITC/propidium iodide (PI) kit (BD Pharmingen). Cells were then analyzed by flow cytometry.

Western blot analysis

At 24 or 48 hours postexposure to the indicated drugs, CHLA20 cells were washed twice with cold PBS and cell lysates collected using RIPA buffer (10 mmol/L Tris pH 7.4, 160 mmol/L NaCl, 5 mmol/L ethylenediaminetetracetic acid, 1% deoxycholate, 1% TritonX-100, 0.1% SDS, 1 mmol/L NaF, and 1 mmol/L Na_3VO_4) plus 1% protease inhibitor cocktail (Roche). After lysates were chilled on ice and pelleted by centrifugation, total protein levels were quantified by Bradford protein assay (Bio-Rad). Proteins in cell lysates (20 μg) were subjected to denaturing electrophoresis, followed by electrotransfer to polyvinylidene difluoride membranes (Bio-Rad). The blots were incubated with the relevant primary antibodies at conditions and concentrations recommended by the manufacturer followed by a 1-hour incubation with the secondary anti-rabbit IgG-HRP antibody (Cell Signaling Technology). The proteins were detected using an enhanced chemiluminescence kit (Perkin Elmer); treated membranes exposed to X-ray film for various exposure times.

Statistical analysis

Synergy was quantified using the CompuSyn software (ComboSyn, Inc.) to calculate the combination index (CI) based on the Chou–Talalay method (25), where $CI < 1$, $CI = 1$, and $CI > 1$ indicate synergistic, additive, and antagonistic effects, respectively. Differences in survival cells between TR100 (or ATM-3507) plus vincristine (or paclitaxel) and plus Z-VAD-FMK were compared using one-way ANOVA followed by Tukey multiple comparison test. Statistical analyses were performed using the software GraphPad Prism 6 (GraphPad Software, Inc.).

Results

Identification of lead compound ATM-3507

We identified ATM-3507 from a library of compounds on the basis of its cytotoxic potency, ability to disrupt Tpm3.1-containing microfilaments and favorable drug-like properties. The goal of the library synthesis project was to improve upon the antitropomyosin activity of TR100 by introducing structural modifications to optimize interactions with the C-terminal domain of tropomyosin Tpm3.1. ATM-3507 retains the three core structural components of TR100, namely an indole scaffold and two binding arms: (1) the "polar arm," which terminates in an ionizable nitrogen atom, and (2) the "nonpolar arm," which is predominantly hydrophobic in nature (Fig. 1 A and B). The nonpolar arm of ATM-3507 is attached to the 5-position of the indole scaffold, as opposed the 3-position on TR100. Furthermore, the nonpolar arm of ATM-3507 is both longer and structurally more complex than that of TR100, with the inclusion of aromatic and amide moieties. While TR100 binds close to the C-terminus of the tropomyosin dimer, the modified nonpolar arm of ATM-3507 is able to make better contact with the helices of the tropomyosin dimer, reaching toward the center of the dimer and interacting with side chains specific for the Tpm3.1 tropomyosin isoform. Relative to the other approximately 200 analogues studied, ATM-3507 consistently showed the most cytotoxic potency against a panel of cancer cell lines (Fig. 2A).

Disruption of Tpm3.1 filaments by ATM-3507

Using a high content imaging (HCI) assay, we found that Tpm3.1-containing filament bundles in SK-N-SH cells were disrupted by 5 μmol/L ATM-3507 (Fig. 2B) with a clear parallel dose-dependent decrease in both cell number and Tpm3.1 filaments (Fig. 2C and D). We used these findings to model the mechanism of action for ATM-3507 (Fig. 2E). We confirmed that ATM-3507 inhibits the ability of Tpm3.1 to protect actin by quantifying polymerized actin over time (Fig. 1F–I) similar to TR100 (26).

Antitropomyosin and antimicrotubule agents induce synergistic cancer cytotoxicity

We previously reported most cancers are enriched for expression of Tpm3.1 relative to other tropomyosin isoforms (12). We tested a panel of neuroblastoma cell lines by Western blot for several tropomyosin isoforms and confirmed Tpm3.1 was expressed in each cell line (Supplementary Fig. S1), suggesting these cells would be suitable models for testing the Tpm3.1 inhibitors. Interestingly, the cell lines differed in their relative expression of Tpm3.1 as well as in the expression of other isoforms.

After determing the IC_{50} concentrations for TR100 and ATM-3507 in each of the neuroblastoma cell lines (Supplementary Table S1), combinations of tropomyosin inhibitors plus vincristine were tested at levels of each drug alone that killed less than 50% of the neuroblastoma cells. We found that the combinations of both tropomyosin inhibitors plus vincristine were completely cytotoxic in CHLA-20 cells (Supplementary Fig. S2A and B). The tropomyosin inhibitors reduced the IC_{50} of vincristine in a dose-dependent fashion in 3 of the 4 cell lines tested (Fig. 3A). All 4 cell lines showed some degree of synergy as determined by

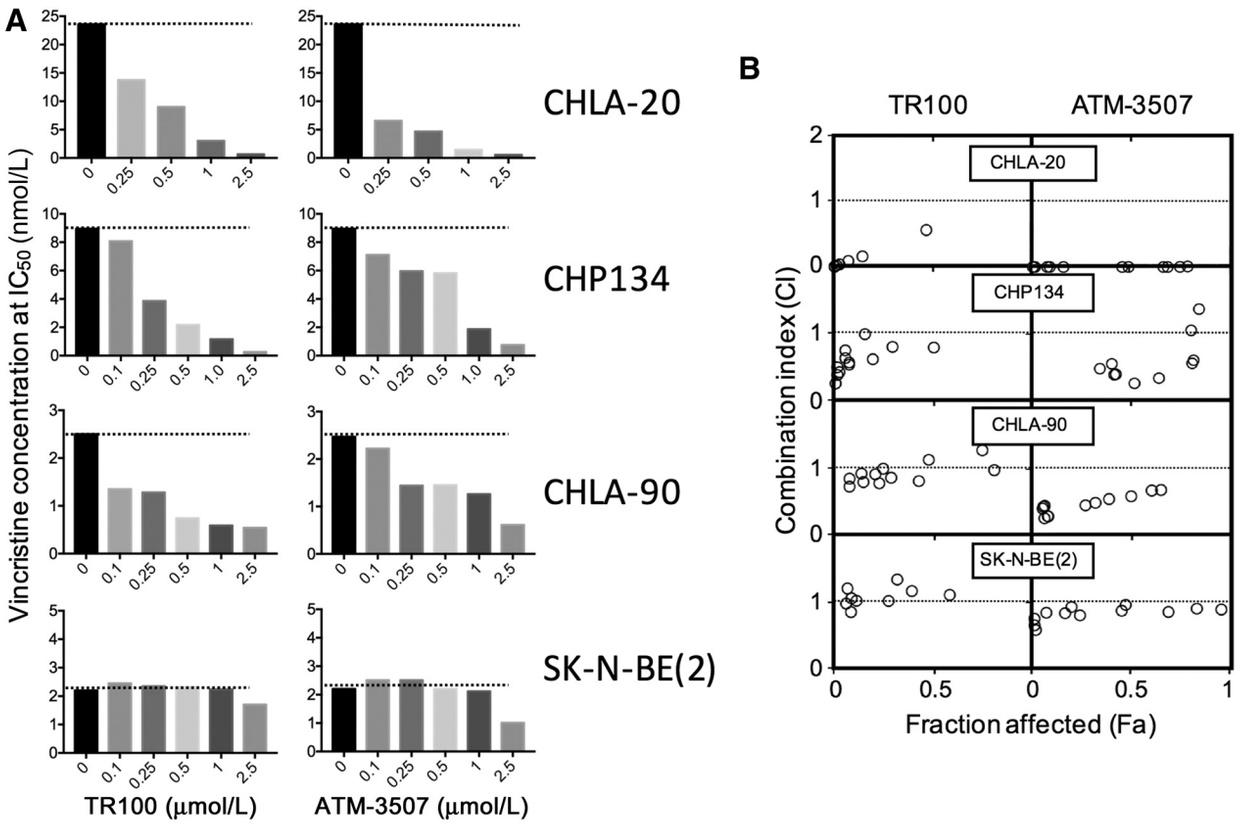

Figure 3.

Effect of combining tropomyosin and microtubule inhibitors on cell growth. **A**, Neuroblastoma cell lines were treated with vincristine alone or combined with TR100 or ATM-3507 and analyzed by MTS assay. Addition of tropomyosin inhibitors reduced the IC_{50} of vincristine in a dose-dependent fashion. **B**, Chou–Talalay analysis of synergy in four neuroblastoma cell lines using various combinations of inhibitors. To determine synergy, concentrations for vincristine (VCR), ATM-3507, and TR100 ranged from one-sixteenth of the IC_{50} to one-half of IC_{50} for each cell line. Values below a combination index of 1 suggest synergy.

the Chou–Talalay method (Fig. 3B). The effect was not limited to the vinca alkaloids as we observed a similar combination efficacy using paclitaxel plus TR100 or ATM-3507 (Supplementary Fig. S3A and S3B). In contrast, we found only slight synergy when TR100 was combined with doxorubicin (Supplementary Fig. S3C), suggesting the sensitization is specific for antimicrotubule agents. The order of administration had little effect on the synergy (Supplementary Fig. S4).

Targeting both tropomyosins and microtubules increases antitumor efficacy

Prior to commencing all mouse xenograft studies, we conducted a truncated MTD study to determine our starting daily dose. The MTD for TR100 and ATM-3507 was 60 and 150 mg/kg, respectively. We tested the combination of each tropomyosin inhibitor given by daily intraperitoneal injection alone or combined with vincristine in neuroblastoma (CHLA20) xenografts (Fig. 4; Supplementary Fig. S5). We found a significant inhibition of tumor growth and prolongation of animal survival using either combination compared with each monotherapy. The median survival of mice increased from 24 and 30 days for mice treated with TR100 or vincristine, respectively, to more than 49 days for mice treated with the combination. Similarly, the median survival of mice increased from 18 days for mice treated with ATM-3507 to more than 49 days for mice treated with the combination. As ATM-3507 is our the clinical lead, we performed additional *in vivo* efficacy studies using a route of delivery and dosing schedule more reflective of what would be used in the clinic. We found that twice weekly intravenous administration of ATM-3507 also showed combination efficacy (Fig. 4D and E). The impact of each treatment or the combination on body weight was minimal (Supplementary Fig. S6).

Pharmacokinetic study of ATM-3507

We measured drug levels following the intravenous administration of ATM-3507 at 30 mg/kg in Balb/c mice ($n = 3$ per time point). The mean half-life of ATM-3507 was 5.01 hours for the terminal elimination phase. The mean AUC_{0-t} in the plasma was 14,548 ng/h/mL. ATM-3507 C_{max} was 5,758 ng/mL. The observed plasma clearance and volume of distribution at steady state of ATM-3507 was 33.8 mL/min/kg and 7.23 L/kg, respectively. Detailed pharmacokinetic parameters of ATM-3507 following intravenous administration are shown in Supplementary Table S2.

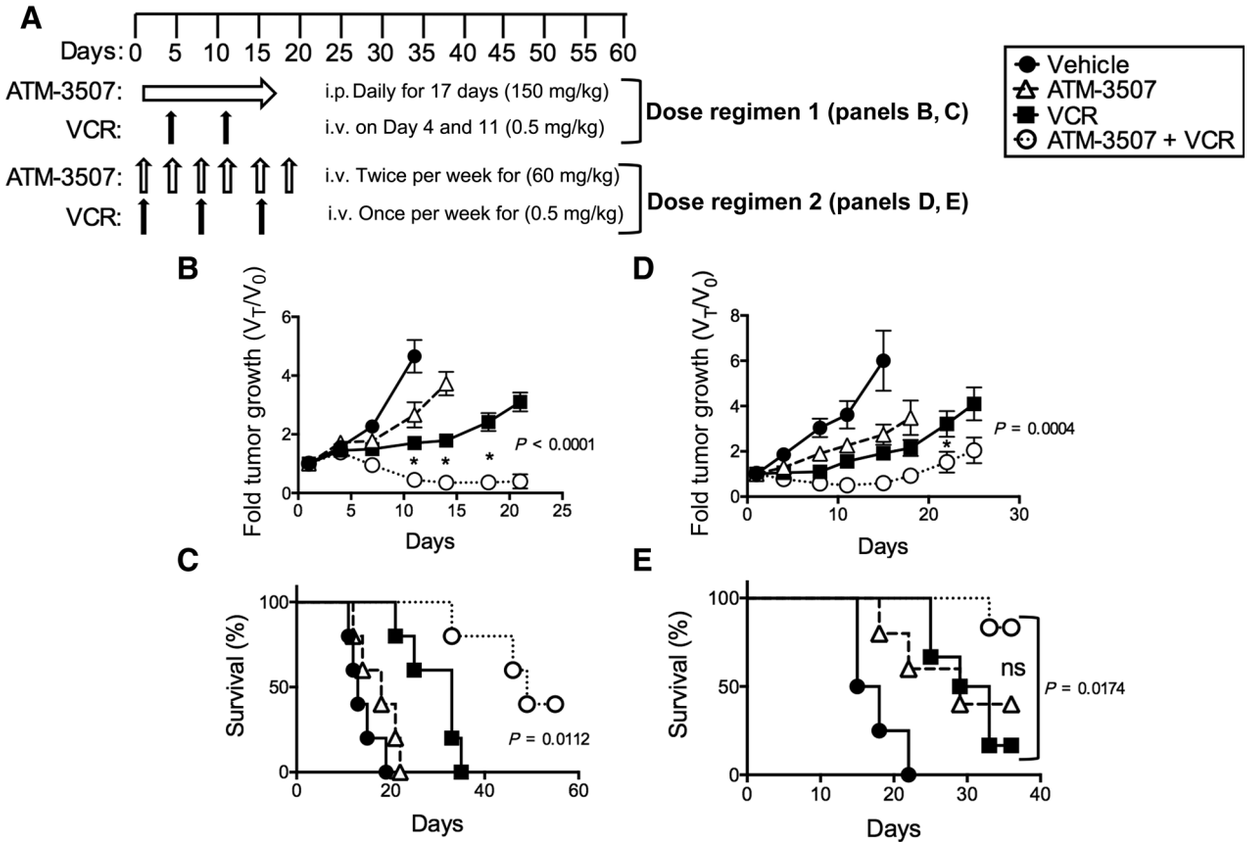

Figure 4.

Effect of combining ATM-3507 and vincristine on tumor growth in athymic nude animals bearing CHLA20 xenografts. **A**, Treatment schemas used for *in vivo* studies. Analysis of tumor growth (**B** and **D**) and animal survival (**C** and **E**) with monotherapies or combinations of intravenous (IV) vincristine with intraperitoneal (IP) ATM-3507 (**B**, **C**; $n = 5$), or intravenous ATM-3507 (**D**, **E**; $n = 4$–6).

The combination of antitropomyosin and antimicrotubule agents induces G_2–M arrest

We investigated the mechanism of action of the drug combination by cell-cycle analysis using flow cytometry following incubation with the drugs for 24 hours. The data were normalized by calculating the percentage of cells in the G_2–M phase as a fraction of the sum of all three cell-cycle phases. Exposing the cell lines with a combination of TR100 or ATM-3507 and vincristine resulted in an increased percentage of cells occupying the G_2–M stage of the cell cycle (Fig. 5A and B). The increase was significant when compared to the percentage of cells in G_2–M induced by each individual drug treatment alone and the vehicle control group. Consistent with these findings, cells showed a significant increase in condensed chromatin (Fig. 5C–G). None of the drug treatments had a detectable impact on interphase microtubule organization (Supplementary Fig. S7). Similarly, low-dose treatment with all agents alone had minimal impact on the organization of the mitotic spindle (Fig. 5I, J, and L). The combinations of TR100 or ATM-3507 with vincristine, however, led to a poorly organized mitotic spindle consistent with a substantial impact on this structure and consequent G_2–M arrest (Fig. 5K and M).

These results are indicative of the mechanism of action of antimicrotubule agents and suggest that inhibiting tropomyosin sensitizes cells to the action of vincristine at substantially lower doses than would normally be required to obtain a G_2–M arrest. This observation suggests that the synergy would lead to cell death via apoptosis.

Antitropomyosins plus antimicrotubule agents induce apoptosis

To determine whether the cytotoxic effect of the combinations of tropomyosin inhibitors and vincristine were due to induction of apoptosis, we measured Annexin-V/PI staining by flow cytometry in CHLA-20 cells treated with TR100 ± vincristine or ATM-3507 ± vincristine. The presence of early and late apoptotic cells increased over time (Fig. 6A and B). This time-dependent increase of apoptotic positive cells was accompanied by time-dependent cleavage of PARP, a product resulting from the proteolytic activity of caspase-3 (Fig. 6C). The combined cytotoxicity was partially prevented by preexposure of cells to the pan-caspase inhibitor Z-VAD-FMK (Fig. 6D). We observed a similar PARP cleavage pattern and partial prevention with the caspase inhibitor in cells exposed to vincristine and ATM-3507 (Fig. 6E and F) as well as TR100 and paclitaxel (Supplementary Fig. S8).

Discussion

We identified a lead drug candidate, ATM-3507, for targeting the Tpm3.1 tropomyosin isoform that is enriched in most cancers.

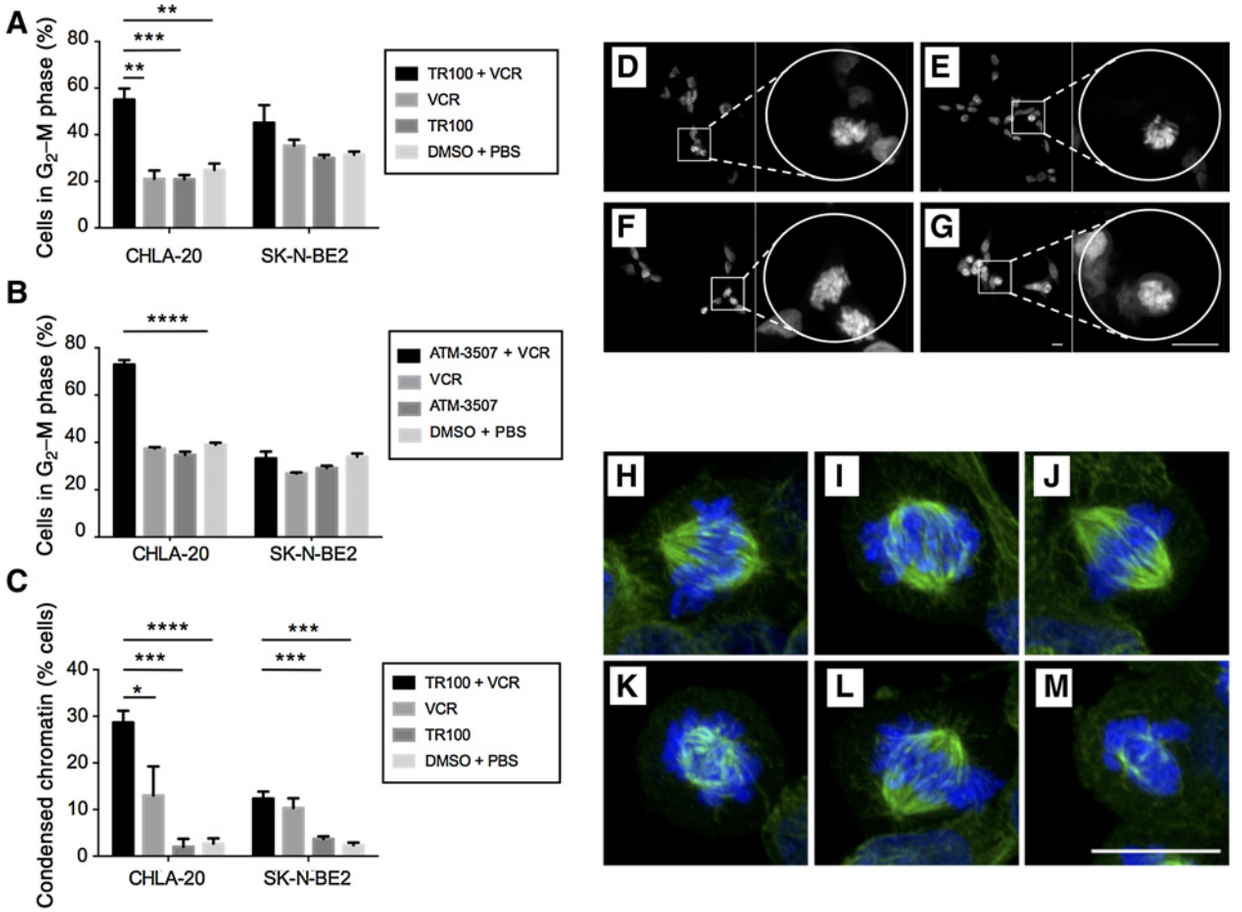

Figure 5.

Effect of combining tropomyosin and microtubule inhibitors on cell cycle, chromatin condensation, and the mitotic spindle. Percentage of cells arrested in G_2–M phase after 24 hours of either single or double drug treatment with TR100 (3.1 μmol/L; **A**) ± vincristine (62.5 nmol/L for CHLA-20; 1.25 nmol/L for SKNBe2) or ATM-3507 (**B**; 4 μmol/L) ± vincristine (10 nmol/L for CHLA-20; 1.5 nmol/L for SKNBe2). Data are presented as a ratio of total cells counted in G_1, S, and G_2–M phase. Error bars represent ± SD. *, $P < 0.05$; **, $P < 0.01$. **C,** Effect of low dose and combined TR100 plus vincristine on chromatin condensation in neuroblastoma cell lines. Combination treatment with low dose TR100 plus vincristine showed a significant increase in condensed chromatin compared with the respective single-drug treatments. Error bars represent ± SD. *, $P < 0.05$; **, $P < 0.01$; ***, $P < 0.001$; ****, $P < 0.0001$. **D–G,** Images of nuclei in CHLA-20 cells with insets showing examples of condensed chromatin. Cells have been treated with vehicle control (**D**), low dose TR100 (**E**), low dose vincristine (**F**), or low dose TR100 plus vincristine (**G**). Scale bars, 10 μm. **H–M,** Images of the mitotic spindle (green) and chromosome organization (blue) in CHLA-20 cells. Cells have been treated with vehicle control (**H**), low dose TR100 (3.1 μmol/L; **I**), low dose vincristine (10 nmol/L; **J**), low dose TR100 plus low dose vincristine (**K**), low dose ATM-3507 (3 μmol/L; **L**), or low dose ATM-3507 plus low dose vincristine (**M**). Scale bar, 10 μm.

ATM-3507 showed cancer cell cytotoxicity comparable with our previously described first-in-class tool compound, TR100. The more highly functionalized structure of ATM-3507 is better able to interact with the C-terminal domain of Tpm3.1, which is predicted to improve selectivity for this particular isoform. ATM-3507 has been shown to be well tolerated in both mouse and dog models with no impact on skeletal muscle studies suggesting that that ATM-3507 can discriminate *in vivo* between the actin cytoskeleton of tumor cells and that of the muscle sarcomere (Novogen Pty Ltd; personal communication). In addition, ATM-3507 lacks the reactive α,β-unsaturated carbonyl moiety present in TR100, a functional group that has been associated with the formation of reactive metabolites (27).

We found a strong synergistic effect when TR100 or ATM-3507 were combined with antimicrotubule agents in both *in vitro* and *in vivo* neuroblastoma models. The observation of profound synergy with antimicrotubule agents suggests that it is based on the structural collaboration of actin filaments containing Tpm3.1 and microtubules. One possibility we considered was a simultaneous impact on both the actin and microtubule cytoskeletons. However, the highly transformed nature of the morphology of the most responsive cells suggests to us that this possibility is less likely. Instead, the cell-cycle analysis and chromosome staining indicates that antitropomyosin drugs sensitize the cell to the mechanism of action of antimicrotubule agents alone (28). Furthermore, the finding that both a vinca alkaloid (vincristine) and a taxane (paclitaxel), which target microtubules via different mechanisms of action (28), can synergize with antitropomyosin agents suggests that there is a specific microtubule–actin filament interaction that plays an important role in G_2–M progression.

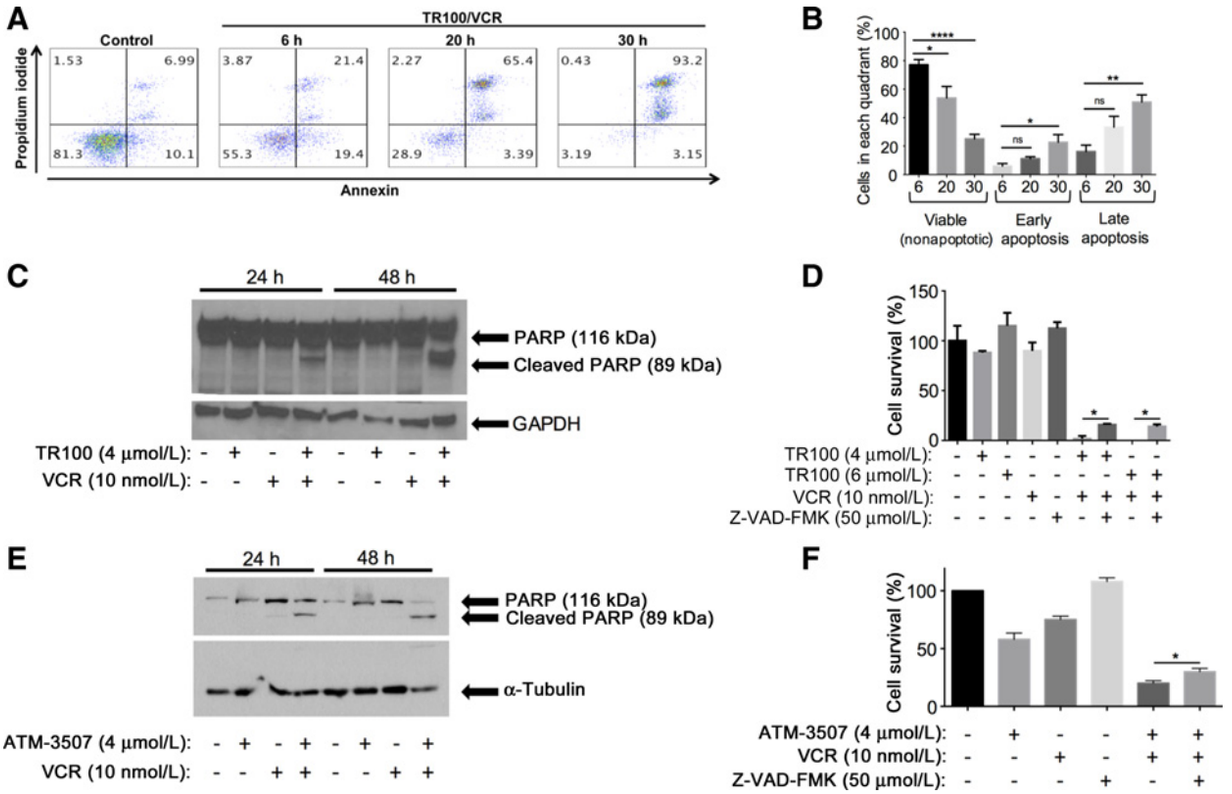

Figure 6.

The combination of tropomyosin inhibitors plus vincristine-induced apoptosis. **A**, CHLA-20 cells were treated with TR100 (4 μmol/L) plus vincristine (10 nmol/L) for 6, 20, and 30 hours, stained with Annexin-V/PI and analyzed by flow cytometry. **B**, Quantitative analysis of $n = 4$ samples show the time-course progression through early and late apoptosis of CHLA-20 cells treated with ATM-3507 (4 μmol/L) plus vincristine (10 nmol/L) for 6, 20, and 30 hours. **C** and **E**, Western blots for showing cleaved PARP only when TR100 (**C**) or ATM-3507 (**E**) were combined with vincristine. **D** and **F,** CHLA-20 cells were pretreated with the pan-caspase inhibitor Z-VAD-FMK (50 μmol/L) for 2 hours prior to treatment with either single treatment (**D**), TR100, or ATM-3507 alone or combined with vincristine and cell survival was determined by MTS at day 3 (**F**).

Indeed, it has previously been demonstrated that reduction in the levels of functional gamma-actin can both suppress microtubule dynamics (29) and contribute to the development of cellular resistance to antimicrotubule agents (30). These observations taken together are consistent with a collaborative role for actin filaments with microtubules in G_2–M progression. This idea is further supported by the recent observation that anti-LIMK compounds synergize with vincristine in a model of neuroblastoma (31). Anti-LIMK compounds have been shown to increase the level of active cofilin, which in turn leads to an increase in cofilin-induced severing of actin filaments (32). While this actin disruption may reflect an effect on Tpm3.1-containing actin filaments, it may also reflect the involvement of more than one type of actin filament population because Tpm3.1-containing actin filaments are highly resistant to severing by cofilin (33). For example, there is evidence that γ-actin plays a role in normal centrosome function (34).

The simplest explanation of the observed synergy is that actin filaments containing Tpm3.1 are involved in the assembly and/or function of the mitotic spindle. The imaging of chromatin disorganization when cells are exposed to both agents suggests that there is a failure of metaphase. This defect could be due to a failure to properly connect the mitotic spindle to the kinetochores. The Drosophila tropomyosin isoform Tm1J is enriched in both centrosomes and the kinetochores throughout metaphase and knockdown of this isoform leads to a G_2–M arrest (35). Because Tm1J is also located in the Golgi, it has been proposed that the impact on the cell cycle could be indirect due to the effect on the Golgi (35). However, it is also possible that the impact on the cell cycle is due to a role for Tm1J in the organization and/or function of the spindle via interaction of microtubules with the kinetochores.

There are also numerous studies implicating actin filaments in normal functioning of the mitotic spindle (36). It has been suggested that cortical actin filaments are required for anchoring and orientation of the mitotic spindle in some mammalian cells (37, 38) possibly via involvement of myosin-10 (37, 39, 40). There is also evidence for an interaction between the actin cortex and astral microtubules (41). We have recently demonstrated an interaction of the microtubule +TIP protein EB1 with γ-actin in the cell cortex which may provide a mechanism for the impact of the actin cytoskeleton on astral microtubules (42). The intrinsic problem with studies that follow actin organization is the difficulty in discerning a specific interaction between actin filaments and the mitotic spindle. It is possible that the ability to follow Tpm3.1-containing actin filaments will allow for the visualization of the relevant actin filament population.

We found synergistic effects in the majority of neuroblastoma cells we tested, which seem to be unrelated to levels of Tpm3.1 expression. How generalizable the synergy will be for other cancer types is not yet known. In addition, whether or not inhibiting tropomyosins might sensitize cancer cells to other therapies is not yet known, although they failed to so with doxorubicin in our experiments. Overall, our results suggests that antitropomyosin compounds should be tested in combination with antimicrotubule agents in a clinical setting once clinical safety data are available for the antitropomyosin lead drug candidate as monotherapy.

Disclosure of Potential Conflicts of Interest

J.R. Stehn has ownership interest (including patents) as a shareholder in Novogen Ltd. H. Treutlein is a consultant/advisory board member for Novogen Ltd. and University of New South Wales. P.W. Gunning is an advisor to the board and member of scientific advisory board (non-executive director of the board), reports receiving a commercial research grant, has ownership interest (including patents), and is a consultant/advisory board member for Novogen Ltd. No potential conflicts of interest were disclosed by the other authors.

Authors' Contributions

Conception and design: M.A. Currier, J.R. Stehn, E. Eiffe, P.W. Gunning, T.P. Cripe

Development of methodology: M.A. Currier, J.R. Stehn, A. Swain, J. Hook, D.W. Eaves, H. Treutlein, I.B. Alieva, T.P. Cripe

Acquisition of data (provided animals, acquired and managed patients, provided facilities, etc.): M.A. Currier, J.R. Stehn, A. Swain, D. Chen, J. Hook, B. Nartker, D.W. Eaves, N. Kloss, J. Zeng, I.B. Alieva, T.P. Cripe

Analysis and interpretation of data (e.g., statistical analysis, biostatistics, computational analysis): J.R. Stehn, A. Swain, D. Chen, J. Hook, E. Eiffe, D.W. Eaves, H. Treutlein, J. Zeng, I.B. Alieva, V.B. Dugina, P.W. Gunning, T.P. Cripe

Writing, review, and/or revision of the manuscript: M.A. Currier, J.R. Stehn, A. Swain, J. Hook, E. Eiffe, I.B. Alieva, V.B. Dugina, E.C. Hardeman, P.W. Gunning, T.P. Cripe

Administrative, technical, or material support (i.e., reporting or organizing data, constructing databases): M.A. Currier, A. Swain, J. Hook, E. Eiffe, B. Nartker, D.W. Eaves, I.B. Alieva

Study supervision: J.R. Stehn, I.B. Alieva, V.B. Dugina, E.C. Hardeman, P.W. Gunning, T.P. Cripe

Grant Support

This work was supported by Novogen as well as grants from The Kids Cancer Project, Oncology Children's Foundation (Sydney, New South Wales, Australia) to T.P. Cripe, E.C. Hardeman, and P.W. Gunning. Funding to support this study was also provided to P.W. Gunning and E.C. Hardeman from the Australian National Health and Medical Research Council and to I.B. Alieva from the Russian Foundation for Basic Research (RFBR grant #15-04-08550) and the MSU Development Program PNR 5.13.

The costs of publication of this article were defrayed in part by the payment of page charges. This article must therefore be hereby marked *advertisement* in accordance with 18 U.S.C. Section 1734 solely to indicate this fact.

Received December 17, 2016; revised March 30, 2017; accepted May 11, 2017; published OnlineFirst May 18, 2017.

References

1. Park JR, Bagatell R, London WB, Maris JM, Cohn SL, Mattay KK, et al. Children's Oncology Group's 2013 blueprint for research: neuroblastoma. Pediatr Blood Cancer 2013;60:985–93.
2. Cohen LE, Gordon JH, Popovsky EY, Gunawardene S, Duffey-Lind E, Lehmann LE, et al. Late effects in children treated with intensive multimodal therapy for high-risk neuroblastoma: high incidence of endocrine and growth problems. Bone Marrow Transplant 2014;49:502–8.
3. Applebaum MA, Henderson TO, Lee SM, Pinto N, Volchenboum SL, Cohn SL. Second malignancies in patients with neuroblastoma: the effects of risk-based therapy. Pediatr Blood Cancer 2015;62:128–33.
4. Helfman DM, Flynn P, Khan P, Saeed A. Tropomyosin as a regulator of cancer cell transformation. Adv Exp Med Biol 2008;644:124–31.
5. Hall A.The cytoskeleton and cancer. Cancer Metastasis Rev 2009;28:5–14.
6. Rao J, Li N. Microfilament actin remodeling as a potential target for cancer drug development. Curr Cancer Drug Targets 2004;4:345–54.
7. Yamaguchi H, Condeelis J. Regulation of the actin cytoskeleton in cancer cell migration and invasion. Biochim Biophys Acta 2007;1773:642–52.
8. Bonello TT, Stehn JR, Gunning PW. New approaches to targeting the actin cytoskeleton for chemotherapy. Future Med Chem 2009;1:1311–31.
9. Gunning PW, Hardeman EC, Lappalainen P, Mulvihill DP. Tropomyosin - master regulator of actin filament function in the cytoskeleton. J Cell Sci 2015;128:2965–74.
10. Stehn JR, Schevzov G, O'Neill GM, Gunning PW. Specialisation of the tropomyosin composition of actin filaments provides new potential targets for chemotherapy. Curr Cancer Drug Targets 2006;6:245–56.
11. Schevzov G, Whittaker SP, Fath T, Lin JJ, Gunning PW. Tropomyosin isoforms and reagents. Bioarchitecture 2011;1:135–64.
12. Stehn JR, Haass NK, Bonello T, Desouza M, Kottyan G, Treutlein H, et al. A novel class of anticancer compounds targets the actin cytoskeleton in tumor cells. Cancer Res 2013;73:5169–82
13. Hill TA, Gordon CP, McGeachie AB, Venn-Brown B, Odell LR, Chau N, et al. Inhibition of dynamin mediated endocytosis by the dynoles–synthesis and functional activity of a family of indoles. J Med Chem 2009;52:3762–73.
14. Eiffe E, Gunning P, Heaton A, Pottabathini N, inventors; Novogen Ltd, assignee. Functionalised and substituted indoles as anti-cancer agents. Australia patent AU2015227454.2015 Jul 16.
15. Greenfield NJ, Kotlyanskaya L, Hitchcock-DeGregori SE. Structure of the N terminus of a nonmuscle alpha-tropomyosin in complex with the C terminus: implications for actin binding. Biochemistry 2009;48:1272–83.
16. Berman HM. The Protein Data Bank: a historical perspective. Acta Crystallogr A 2008;64:88–95.
17. Arnold K, Bordoli L, Kopp J, Schwede T. The SWISS-MODEL workspace: a web-based environment for protein structure homology modelling. Bioinformatics 2006;22:195–201.
18. Smith DK, Treutlein HR, Maurer T, Owczarek CM, Layton MJ, Nicola NA, et al. Homology modelling and 1H NMR studies of human leukaemia inhibitory factor. FEBS Lett 1994;350:275–80.
19. Phillips JC, Braun R, Wang W, Gumbart J, Tajkhorshid E, Villa E, et al. Scalable molecular dynamics with NAMD. J Comput Chem 2005;26:1781–802.
20. Zeng J, Treutlein HR. A method for computational combinatorial peptide design of inhibitors of Ras protein. Protein Eng 1999;12:457–68.
21. Lee C, Yang W, Parr RG. Development of the Colle-Salvetti correlation-energy formula into a functional of the electron density. Phys Rev B Condens Matter 1988;37:785–9.
22. Becke AD.Density-functional exchange-energy approximation with correct asymptotic behavior. Phys Rev A Gen Phys 1988;38:3098–100.
23. Krishnan R, Binkley JS, Seeger R, Pople JA. Self-consistent molecular orbital methods. XX. A basis set for correlated wave functions. J Chem Phys 1980;72:650–4.
24. Vindin H, Bischof L, Gunning P, Stehn J. Validation of an algorithm to quantify changes in actin cytoskeletal organization. J Biomol Screen 2014;19:354–68.
25. Chou TC.Drug combination studies and their synergy quantification using the Chou-Talalay method. Cancer Res 2010;70:440–6.
26. Bonello TT, Janco M, Hook J, Byun A, Appaduray M, Dedova I, et al. A small molecule inhibitor of tropomyosin dissociates actin binding from tropomyosin-directed regulation of actin dynamics. Sci Rep 2016;6:19816.
27. Benigni R, Bossa C. Mechanisms of chemical carcinogenicity and mutagenicity: a review with implications for predictive toxicology. Chem Rev 2011;111:2507–36.

28. Mukhtar E, Adhami VM, Mukhtar H. Targeting microtubules by natural agents for cancer therapy. Mol Cancer Ther 2014;13:275–84.
29. Po'uha ST, Honore S, Braguer D, Kavallaris M. Partial depletion of gamma-actin suppresses microtubule dynamics. Cytoskeleton 2013;70:148–60.
30. Verrills NM, Po'uha ST, Liu ML, Liaw TY, Larsen MR, Ivery MT, et al. Alterations in gamma-actin and tubulin-targeted drug resistance in childhood leukemia. J Natl Cancer Inst 2006;98:1363–74.
31. Mardilovich K, Baugh M, Crighton D, Kowalczyk D, Gabrielsen M, Munro J, et al. LIM kinase inhibitors disrupt mitotic microtubule organization and impair tumor cell proliferation. Oncotarget 2015;6:38469–86.
32. He L, Seitz SP, Trainor GL, Tortolani D, Vaccaro W, Poss M, et al. Modulation of cofilin phosphorylation by inhibition of the Lim family kinases. Bioorg Med Chem Lett 2012;22:5995–8.
33. Bryce NS, Schevzov G, Ferguson V, Percival JM, Lin JJ, Matsumura F, et al. Specification of actin filament function and molecular composition by tropomyosin isoforms. Mol Biol Cell 2003;14:1002–16.
34. Po'uha ST, Kavallaris M. Gamma-actin is involved in regulating centrosome function and mitotic progression in cancer cells. Cell Cycle 2015;14:3908–19.
35. Goins LM, Mullins RD. A novel tropomyosin isoform functions at the mitotic spindle and Golgi in Drosophila. Mol Biol Cell 2015;26:2491–504.
36. Sandquist JC, Kita AM, Bement WM. And the dead shall rise: actin and myosin return to the spindle. Dev Cell 2011;21:410–9.
37. Toyoshima F, Nishida E. Integrin-mediated adhesion orients the spindle parallel to the substratum in an EB1- and myosin X-dependent manner. EMBO J 2007;26:1487–98.
38. Thery M, Racine V, Pepin A, Piel M, Chen Y, Sibarita JB, et al. The extracellular matrix guides the orientation of the cell division axis. Nat Cell Biol 2005;7:947–53.
39. Weber KL, Sokac AM, Berg JS, Cheney RE, Bement WM. A microtubule-binding myosin required for nuclear anchoring and spindle assembly. Nature 2004;431:325–9.
40. Hirano Y, Hatano T, Takahashi A, Toriyama M, Inagaki N, Hakoshima T. Structural basis of cargo recognition by the myosin-X MyTH4-FERM domain. EMBO J 2011;30:2734–47.
41. Fink J, Carpi N, Betz T, Betard A, Chebah M, Azioune A, et al. External forces control mitotic spindle positioning. Nat Cell Biol 2011;13:771–8.
42. Dugina V, Alieva I, Khromova N, Kireev I, Gunning PW, Kopnin P. Interaction of microtubules with the actin cytoskeleton via cross-talk of EB1-containing +TIPs and gamma-actin in epithelial cells. Oncotarget 2016;7:72699–715.